THE JOURNAL OF PHYSICAL CHEMISTRY C
A JOURNAL OF THE AMERICAN CHEMICAL SOCIETY

pubs.acs.org/JPCC

Article

Structure and Connectivity in an Amorphous Silicon Oxycarbide Polymer-Derived Ceramic: Results from 2D ^{29}Si NMR Spectroscopy

Published as part of The Journal of Physical Chemistry virtual special issue "Hellmut Eckert Festschrift".

Ivan Hung, Emanuel Ionescu, Jishnu Sen, Zhehong Gan, and Sabyasachi Sen*

Cite This: *J. Phys. Chem. C* 2021, 125, 4777−4784

Read Online

ACCESS | Metrics & More | Article Recommendations

ABSTRACT: The atomic structure of the Si−O−C tetrahedral network of an amorphous silicon oxycarbide polymer-derived ceramic (PDC) of the composition $SiO_{0.94\pm0.11}C_{1.13\pm0.08}$ was studied at both the short range and the intermediate range using 1D and 2D ^{29}Si nuclear magnetic resonance (NMR) spectroscopic techniques, respectively . The 1D ^{29}Si magic angle-spinning NMR spectrum of the PDC indicates that the Si−O−C network consists of SiO_4, SiO_3C, SiO_2C_2, and SiC_4 units with relative abundances of approximately 26, 25, 20, and 29%, respectively. The 2D ^{29}Si extended CSA amplification spectrum of this PDC shows that the chemical shift anisotropy (Δ) of the mixed-bond SiO_xC_{4-x} units is significantly higher than that of the SiO_4 units. On the other hand, the unusually high Δ-value for the SiC_4 units was interpreted to be indicative of its role as the connecting element between the Si−O−C network and the free-carbon nanodomains. The 2D ^{29}Si double-quantum correlation NMR spectrum of this PDC indicates that there is extensive direct linking between SiO_4 and SiO_3C units in the Si−O−C network besides the connectivity between like SiO_xC_{4-x} units, while the SiO_4 and SiO_2C_2 units are only linked via a SiO_3C unit. In contrast, the SiO_3C units show no restriction in linking with the other SiO_xC_{4-x} units in the network. Finally, the SiC_4 units show significant clustering, which is consistent with their spatial localization at the interface between the Si−O−C network and the sp^2 C nanodomains. Such a spatial distribution of the SiO_xC_{4-x} units is argued to be consistent with their mass-fractal dimensions measured in previous studies.

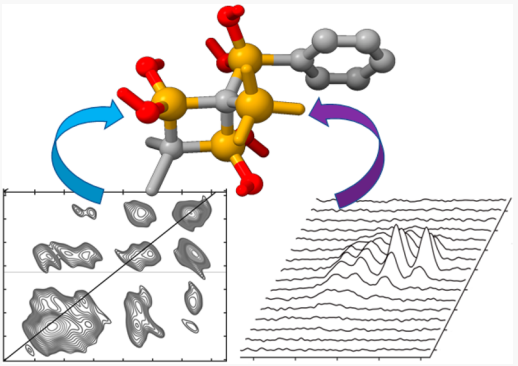

INTRODUCTION

Polymer-derived ceramics (PDCs) are a class of amorphous materials that are typically synthesized by the pyrolysis of Si-based preceramic polymers. PDCs in Si−B−C−O and Si−B−C−N systems are technologically promising due to their remarkable thermomechanical stability that can be combined with an intriguingly wide range of attributes, including high electrical conductivity, bioactivity, and optoelectronic properties.[1−8] A fundamental understanding of the relationship between these properties and the atomic structure of PDCs is of key importance in the engineering of these materials for specific applications. In this regard, the ternary Si−O−C and Si−C−N PDCs serve as model systems, with their structures characterized by a network of corner-sharing SiO_xC_{4-x} and SiN_xC_{4-x} ($0 \le x \le 4$) tetrahedra, respectively, that coexist with nanodomains of sp^2-hybridized amorphous carbon.[1−4,8−10] A wide variety of characterization techniques have been used over the last two decades to investigate the structure of these PDCs at various length scales.[1−18] In particular, ^{29}Si and ^{13}C magic angle-spinning nuclear magnetic resonance (MAS NMR) spectroscopy have played an important role in the identification and quantitation of the mixed-bonded SiO_xC_{4-x} or SiN_xC_{4-x} units and C in the sp^2 or sp^3 bonding mode in the structure.[1−4,6,9,10] The relative fractions of these mixed-bonded tetrahedral units, at least in PDCs pyrolyzed at temperatures above 1000 °C, suggest a partial avoidance of the bonding between the oxygen (nitrogen)-rich and carbon-rich SiO_xC_{4-x} (SiN_xC_{4-x}) tetrahedral units, and consequently a spatial segregation of these units, in the SiOC (SiCN) tetrahedral networks. The avoidance of bonding between C and O (N) atoms in these PDCs implies that the SiO_4 (SiN_4) and SiC_4 tetrahedra cannot be directly connected to each other.

It may be noted in this regard that two distinctly different scenarios of intertetrahedral connectivity have been put forward in the literature.[12,13,15,16] In one scenario, the free carbon is present in nanodomains as dispersed graphene or

Received: November 1, 2020
Revised: February 4, 2021
Published: February 17, 2021

turbostratic graphite, which is embedded in a matrix of a fully connected network of corner-shared SiO_xC_{4-x} tetrahedra.[12,15] In a second model based on small-angle X-ray scattering studies, the structure of SiOC PDCs was proposed to consist of a cellular network of free carbon, with nanodomains of silica sequestered within the cells.[13,16] While the silica nanodomains consist predominantly of corner-shared SiO_4 tetrahedra, the domain walls at the interface between these nanodomains and the carbon network consist primarily of carbon-rich SiO_xC_{4-x} tetrahedra. For each model, the characteristic length scale of the nanodomains was proposed to be on the order of a few nanometers. In the second model, the silica-rich domains were a few nanometers in diameter, while the thickness of the domain walls was on the order of ∼1 nm. These structural models aside, a number of physical properties of SiOC PDCs are consistent with the presence of two interpenetrating continuous networks, one of which is silica-rich and the other of which is carbon-rich.

Recent ^{29}Si NMR spin−lattice relaxation (SLR) studies of SiOC PDCs indicated that the constituent SiO_xC_{4-x} tetrahedral units form a network such that the spatial distribution of these units or their mass M scales with distance R as $M \sim R^{D_f}$, with the fractal dimension D_f being substantially smaller ($2.0 \leq D_f \leq 2.5$) than the embedding Euclidean dimension of 3.[9] It was hypothesized that the mixed coordination of Si, i.e., the presence of both C and O atoms as the nearest neighbors of the Si atoms combined with the absence of any carbon−oxygen bonding, could lead to steric hindrance in the way of the efficient packing of the SiO_xC_{4-x} units and consequently to the mass-fractal character of the SiOC network.[9,19] However, the connectivity between the mixed-bonded tetrahedral units, which is believed to be of crucial importance in controlling the thermodynamic stability of these PDCs, remains poorly understood to date.[10] As noted above, the distinctive ^{29}Si and ^{13}C NMR isotropic chemical shifts δ_{iso} have allowed the identification and quantitation of various Si and C environments in SiOC PDCs. However, besides the δ_{iso} of a nuclide, which is characteristic of its coordination environment, the chemical shift anisotropy (CSA) carries important complementary information related to the symmetry of the local electronic environment of a nuclide and, in combination with δ_{iso}, can often be useful in deciphering the intermediate-range order in a glass structure beyond the nearest-neighbor length scale.[18−21] Chemical shift is a a second-rank tensor with principal components δ_{xx}, δ_{yy}, and δ_{zz} such that $|\delta_{zz} - \delta_{iso}| \geq |\delta_{xx} - \delta_{iso}| \geq |\delta_{yy} - \delta_{iso}|$. Therefore, the δ_{iso} is defined as

$$\delta_{iso} = \frac{1}{3}(\delta_{xx} + \delta_{yy} + \delta_{zz})$$

On the other hand, the CSA is characterized by the anisotropy Δ and the asymmetry parameter η ($0 \leq \eta \leq 1$), which are defined as

$$\Delta = \delta_{zz} - \delta_{iso}$$

$$\eta = \frac{\delta_{yy} - \delta_{xx}}{\delta_{zz} - \delta_{iso}}$$

The parameters Δ and η represent the deviation of the tensor from spherical and uniaxial symmetries, respectively. However, the CSA of the corner-shared tetrahedral Si environments in PDCs is expected to be rather small and thus difficult to accurately estimate from simple one-dimensional (1D) NMR spectra, especially in the presence of multiple center bands that cover a wide range of δ_{iso} in the 1D spectrum. Recent studies have shown that in such situations two-dimensional (2D) CSA amplification NMR methods, such as xCSA, can be successfully employed to accurately determine small Δ values of less than 10 ppm.[24,25] Here, we report for the first time the application of 2D ^{29}Si xCSA NMR spectroscopy to determine the ^{29}Si CSA parameters of the various SiO_xC_{4-x} units in a SiCO PDC, which are then compared to the ^{29}Si NMR chemical shift tensor parameters calculated on molecular fragments using density functional theory (DFT). In addition, the connectivity between the SiO_xC_{4-x} units in this PDC is determined using 2D ^{29}Si double-quantum (DQ) correlation NMR spectroscopy, where the spatial proximity information is generated through a homonuclear dipolar recoupling sequence. These results are used to build a comprehensive structural model of the intermediate-range order in SiOC PDCs.

METHODS

Sample Synthesis and Chemical Analysis. The SiOC PDC sample used in this study was synthesized using commercially available polysiloxane SPR-212 (Starfire Systems Inc., NY, USA). The polymer was cross-linked in an alumina tube furnace at 250 °C for 2 h under a flowing argon atmosphere. Subsequently, the cross-linked sample was pyrolyzed in an alumina-tube furnace at 1100 °C (heating rate of 100 °C/h, Ar atmosphere) for 2 h. The chemical composition of the sample was determined in triplicate using a carbon analyzer Leco-200 (Leco Corporation, St. Joseph, MI, USA) and a N/O analyzer Leco TC-436 (Leco Corporation, St. Joseph, Michigan, USA). The silicon weight fraction was calculated as the difference to 100 wt % assuming that no other elements were present in the samples. The analyzed composition of the sample was then calculated as $SiO_{0.94\pm0.11}C_{1.13\pm0.08}$.

^{29}Si NMR Spectroscopy. All ^{29}Si NMR spectra of the SiOC PDC sample, with the ^{29}Si nuclide in natural abundance, were collected at the National High Magnetic Field Laboratory (NHMFL) in Tallahassee, FL, USA using a 31 mm bore 19.6 T magnet equipped with a Bruker Avance NEO console operating at the resonance frequency for ^{29}Si of 165.2 MHz. Carr−Purcell Meiboom−Gill (CPMG) multiple-echo acquisition was used for the signal enhancement of all spectra, where the time-domain echoes were summed during processing.[26] A low-E double-resonance 3.2 mm MAS probe designed and built at the NHMFL[27] was used for the 1D MAS and 2D double-quantum (DQ) correlation spectra, with $\pi/2$- and π-pulses of 4 and 8 μs, respectively, a rf field of 62.5 kHz, spectral widths of 100 kHz, and a MAS frequency ν_r = 12 kHz. The 1D ^{29}Si MAS spectrum was acquired with 60 CPMG loops of ∼2 ms echo acquisition windows, a recycle delay of 10 s, and 2048 scans, resulting in a total experimental time of ∼6 h. Spectra collected with different recycle delays indicated the absence of any differential relaxation. The 2D ^{29}Si DQ correlation spectra were acquired with 163 CPMG loops of ∼1 ms echo acquisition windows, a recycle delay of 30 s, 640 scans, an indirect spectral width of 24 kHz, and 12 complex t_1 points, resulting in a total experimental time for each spectrum of ∼129 h. ^{29}Si DQ coherences were generated using the symmetry-based $SR26_4^{11}$ sequence[28] with a rf field of 78 kHz (6.5× the MAS frequency) and durations for DQ excitation and reconversion of τ = 6.7 and 9.3 ms for the two different spectra. Hypercomplex 2D acquisition was performed using

https://dx.doi.org/10.1021/acs.jpcc.0c09860
J. Phys. Chem. C 2021, 125, 4777−4784

the States method[29] on the DQ excitation segment of the pulse sequence. The 2D ^{29}Si extended CSA amplification (xCSA) spectrum[24] was acquired with a single-resonance 7.0 mm MAS probe designed and built at the NHMFL, $\pi/2$- and π-pulses of 5.9 and 11.8 μs, respectively, a rf field of 42.4 kHz, a spectral width of 100 kHz, a MAS frequency ν_r = 6 kHz, 72 CPMG loops of ~2 ms echo acquisition windows, a recycle delay of 27 s, 160 scans, and 16 complex t_1 points, resulting in a total experimental time of ~39 h. The xCSA sequence employed 7 π-pulses that spanned four rotor periods to disrupt the averaging of the CSA by MAS and efficiently amplify it by a factor of κ = 6, i.e., the spinning sideband intensities along the indirect dimension appear as if the MAS frequency is 6× lower than that applied. In the current instance, the observed CSA is equivalent to that which would be observed at 1 kHz MAS. Evolution along the indirect dimension spans one rotor period τ_r, i.e., t_1 = [0, τ_r], and the resulting spectral width in the indirect dimension is equal to the number of complex t_1 points multiplied by $\nu_r/6$. Hypercomplex 2D acquisition was performed using the States method simultaneously on the phases of the CPMG π-pulses and the receiver.[22,23,27] Processing of the xCSA indirect dimension was performed without first-point scaling, apodization, or zero-filling, which resulted in 16 discrete points that corresponded to CSA spinning sideband intensities.

DFT Calculation of ^{29}Si NMR Parameters. The ^{29}Si NMR chemical shift tensor parameters for the relevant SiO_xC_{4-x} units were calculated using the gauge-including projector augmented wave (GIPAW) method based on DFT.[30] The GIPAW method relies on the reconstruction of the all-electron magnetic response from the pseudowave functions and can be used to calculate the NMR parameters for a wide variety of nuclides with good accuracy.[30] The NMR calculations in this study were carried out on molecular fragments containing the relevant SiO_xC_{4-x} units after their geometry optimizations (Figure 1). These molecular fragments were hydrogen--terminated using $-SiH_3$ groups (see Figure 1). These molecular fragments were placed inside a 20 Å cubic cell with periodic boundary conditions, and a geometry optimization and NMR calculations were carried out using the codes CASTEP and CASTEP-NMR (Biovia Inc.), respectively, within the generalized gradient approximation with PBE XC functionals, on-the-fly-generated ultrasoft pseudopotentials, and plane wave basis sets with an energy cutoff of 610 eV. These calculations yielded the absolute shielding tensor principal components σ_{xx}, σ_{yy}, and σ_{zz}. The isotropic chemical shift δ_{iso} was obtained from the isotropic shielding σ_{iso} = 1/3(σ_{xx}+ σ_{yy}+ σ_{zz}) using the relationship $\delta_{iso} = -(\sigma_{iso} - \sigma_{ref})$, where σ_{ref} is the isotropic shielding of a reference material. The crystalline SiO_2 polymorph α-quartz was used as a reference in this study, and the calculated ^{29}Si σ_{iso} = 429 ppm was equated to the experimental value of ^{29}Si δ_{iso} = −107 ppm.

RESULTS AND DISCUSSION

The 1D ^{29}Si CPMG MAS NMR spectrum of the PDC sample collected at an MAS frequency of 12 kHz is shown in Figure 2. This spectrum reveals four well-resolved peaks centered at −107, −71, −33, and −10 ppm, which can be readily assigned to SiO_4, SiO_3C, SiO_2C_2, and SiC_4 units, respectively, based on previous studies.[1,9] The simulation of this spectrum with Gaussian peaks yielded relative fractions of the SiO_4, SiO_3C, SiO_2C_2, and SiC_4 structural units from the corresponding peak areas as approximately 26, 25, 20, and 29%, respectively, within an uncertainty of ±3% (Figure 2). These relative concentrations of various SiO_xC_{4-x} units were used to calculate the chemical composition of this PDC under the assumptions of

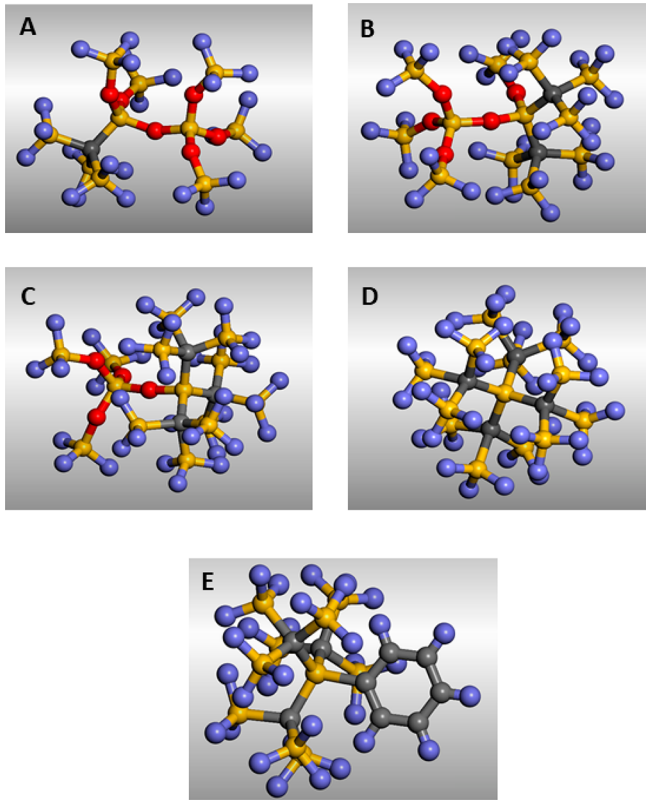

Figure 1. Geometry-optimized molecular fragments used to calculate ^{29}Si NMR parameters for various SiO_xC_{4-x} units. Si, O, C, and H are shown in yellow, red, gray, and blue, respectively. (A) SiO_4 and SiO_3C units linked via oxygen and terminated with $-SiH_3$ groups, (B) SiO_4 and SiO_2C_2 units linked via oxygen and terminated with $-SiH_3$ groups, (C) SiO_4 and $SiOC_3$ units linked via oxygen and terminated with $-SiH_3$ groups, (D) the central SiC_4 unit terminated with $-SiH_3$ groups, and (E) the central SiC_4 unit terminated with three $-SiH_3$ groups and a C_6H_5 ring.

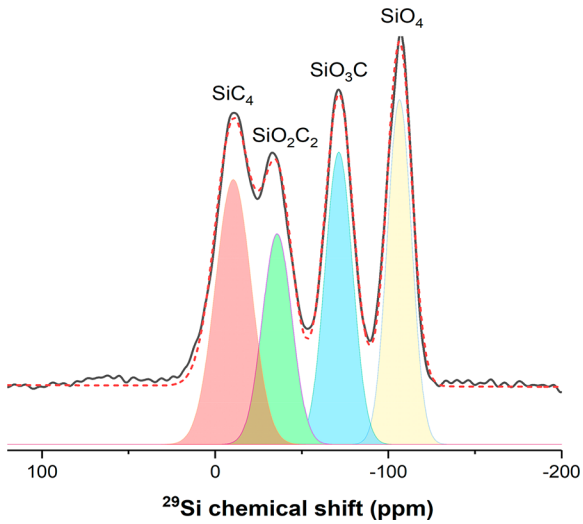

Figure 2. Experimental (solid black line) and simulated (red dashed line) ^{29}Si MAS spectra of the SiOC PDC sample. Individual Gaussian simulation components corresponding to SiO_4, SiO_3C, SiO_2C_2, and SiC_4 units are shown in yellow, cyan, green, and red, respectively.

https://dx.doi.org/10.1021/acs.jpcc.0c09860
J. Phys. Chem. C 2021, 125, 4777−4784

(1) the complete absence of any carbon−oxygen bonds, (2) tetrahedral coordination for Si and C atoms in the network, and (3) that each oxygen is bonded to two Si atoms. The resulting composition of the SiOC network from ^{29}Si NMR is thus $SiO_{1.09\pm0.08}C_{0.45\pm0.03}$, which is consistent with the chemically analyzed composition of $SiO_{0.94\pm0.11}C_{1.13\pm0.08}$ in terms of the Si/O ratio and yields a free-carbon content of 0.68 ± 0.08 atoms of C per Si atom in the structure. It is noteworthy that the width of the peak corresponding to the SiC_4 unit is ∼2.1−2.5 ppm wider than those for the SiO_3C and SiO_2C_2 units, which may suggest the composite nature of the SiC_4 peak and the possible presence of $SiOC_3$ units. However, a recent ^{29}Si NMR study has indicated the lack of any detectable fraction of $SiOC_3$ units in a SiOC PDC obtained from the same precursor, which was pyrolyzed at 600 °C.[31] Therefore, it is likely that the relative fraction of these units in the SiOC PDC sample used in the present study is also rather small, and their role in the connectivity of the network can be safely ignored. Indeed, a comparison between the Si/O ratios obtained from the chemical analysis and from ^{29}Si NMR provides an upper bound for the concentration of the $SiOC_3$ units in this PDC of ∼8%. This result is consistent with the observation in the literature that the typical range for the relative fraction of $SiOC_3$ units in SiOC PDCs is only ∼2−5%. Finally, the relative fractions of the various SiO_xC_{4-x} units in this PDC as obtained from ^{29}Si NMR can be compared to those expected from a random distribution of Si−O and Si−C bonds in the network. The latter can be obtained from the following expression:[9]

$$P(SiO_xC_{4-x}) = \frac{4!}{x!(4-x)!}(p_{Si-O})^x(p_{Si-C})^{4-x}$$

In this expression, $P(SiO_xC_{4-x})$ is the probability of finding any SiO_xC_{4-x} unit, while p_{Si-O} and p_{Si-C} are the probabilities of finding a Si−O and Si−C bond, respectively, in the network. Since every O atom is bonded to two Si atoms in the network, p_{Si-O} = 0.5*(O/Si), and p_{Si-C} is given simply by 1 − (p_{Si-O}). Therefore, for the PDC sample used in this study, the NMR-derived value of O/Si = 1.09 predicts only ∼8.8% SiO_4 units from a random distribution model, which is substantially smaller than the observed value from ^{29}Si MAS NMR of ∼26%. This result directly implies the significant spatial segregation and clustering of the oxygen-rich and carbon-rich SiC_xO_{4-x} units in the SiOC network of this PDC.

The 2D ^{29}Si xCSA/CPMG spectrum of the PDC sample is shown in Figure 3. A projection along the isotropic dimension

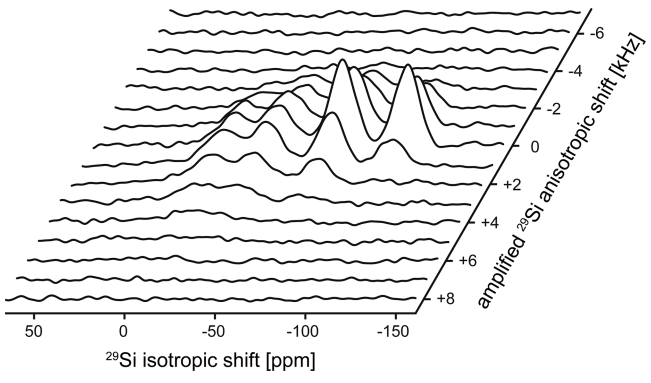

Figure 3. Stacked plot of the 2D ^{29}Si xCSA spectrum of the SiOC PDC sample.

(not shown) is consistent with the MAS spectrum in Figure 2, while the anisotropic dimension provides CSA information for each site that is magnified sixfold in this spectrum. The simulation of these spinning sideband manifolds along the anisotropic dimension (Figure 4) was carried out using a Gaussian distribution of δ_{xx}, δ_{yy}, and δ_{zz} with a full-width at half-maximum of 12−14 ppm to account for the structural disorder characteristic of an amorphous material. The results of these simulations indicate that all Si sites are characterized by rather small |Δ| values, ranging from 13 ppm for the SiO_4 sites to 23 ppm for the SiO_2C_2 and SiC_4 units. The asymmetry parameter η for all sites ranged between 0.5 and 0.8 (Table 1). These chemical shift tensor parameters are compared in Table 1 with those calculated on the molecular fragments using the GIPAW method. The calculated δ_{iso} values for various Si sites show rather good agreement with the experimental values. It may be noted here that in a previous study similar values of ^{29}Si δ_{iso} were obtained from the GIPAW method-based calculations on three-dimensionally extended structural models of Si-oxycarbide networks.[32] It was shown in that study[32] that the ^{29}Si δ_{iso} for the SiO_xC_{4-x} units was strongly correlated to the average Si−O−Si angles, but no clear correlation was observed between the former and the Si−C bond length. These results indicate that the ^{29}Si δ_{iso} for a SiO_xC_{4-x} unit is primarily controlled by its nearest-neighbor environment, and the structure beyond this length scale does not significantly affect this NMR parameter, thus justifying the termination scheme for the molecular fragments used in the present study. Here we also report the calculated Δ-and η-values for the various SiO_xC_{4-x} units and compare them to the experiment (Table 1). The calculated Δ-values for these units vary within a relatively narrow range and display the same trend as that in the experiment for SiO_4, SiO_3C, and SiO_2C_2 units (Table 1). On the other hand, the calculated Δ-value for the SiC_4 unit connected to four next-nearest neighbor Si atoms shows a significant departure from the observed experimental trend, although the former is in good agreement with the experimental and calculated values for crystalline polymorphs of SiC.[33] The relatively high ^{29}Si Δ-value that was experimentally observed for the SiC_4 units is also inconsistent with that calculated for the $SiOC_3$ units (Table 1) and is likely indicative of the connectivity of the SiC_4 units to the sp^2 C atoms at the interface between the SiOC network and the amorphous C domains. Such a connectivity would significantly lower the local symmetry of the bonding environment of these units, which could manifest in an increase in the ^{29}Si Δ-value. This hypothesis is supported by the results of DFT calculations of the chemical shift tensor parameters of a SiC_4 unit connected to three nearest-neighbor Si atoms and a C that is part of a six-membered C-ring (Figure 1). The calculated δ_{iso} for this "asymmetric" SiC_4 unit is not significantly different from that calculated for the "symmetric" SiC_4 unit connected to four next-nearest neighbor Si atoms (Table 1). However, the calculated Δ- and η-values for the asymmetric unit are rather similar to those determined experimentally for the SiC_4 unit (Table 1).

The 2D ^{29}Si double-quantum vs single-quantum (DQ-SQ) correlation spectra collected at a spinning speed of 12 kHz is shown in Figure 5 after being sheared into a SQ−SQ correlation representation. Although previous studies[28] have shown that such spectra for long recoupling times (>10 ms) can provide information on ^{29}Si spin pairs separated by up to 8 Å, the spectra collected in the present study with short

https://dx.doi.org/10.1021/acs.jpcc.0c09860
J. Phys. Chem. C 2021, 125, 4777−4784

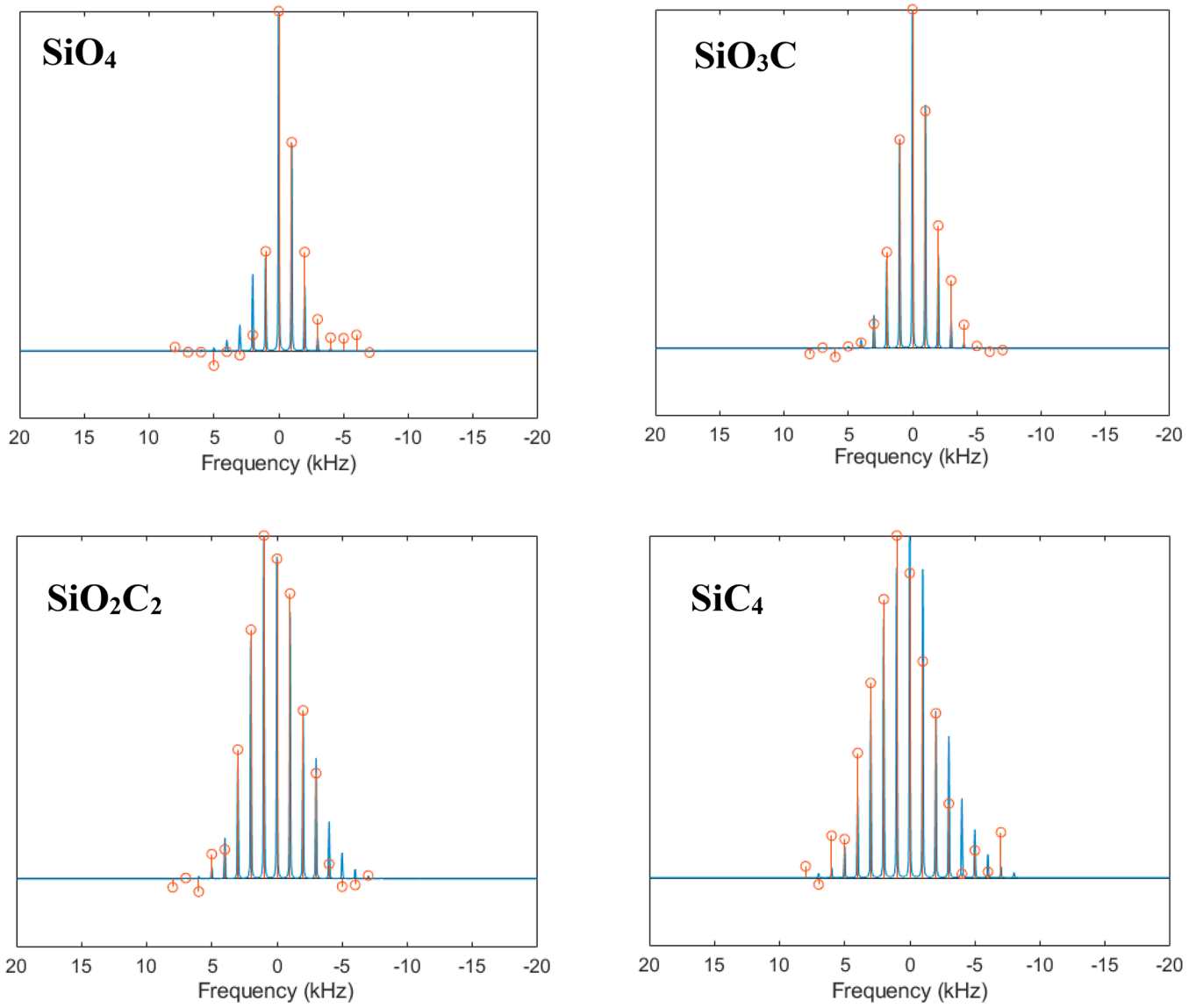

Figure 4. Representative experimental ^{29}Si NMR anisotropic spinning sideband spikelet patterns (orange lines and circles) for SiO_4, SiO_3C, SiO_2C_2, and SiC_4 units. Anisotropic slices for these sites were taken along the F1 dimension at the maximum for each peak. Corresponding simulations are shown as blue lines.

Table 1. Experimental (In Bold) And Calculated (In Parentheses) ^{29}Si Chemical Shift Tensor Parameters for Various SiO_xC_{4-x} Units

structural units	δ_{iso} (ppm)	average Δ (ppm)	average η
SiO_4	**−107** (−110)	**−12** (−10)	**0.5** (0.2)
SiO_3C	**−71** (−73)	**−16** (−30)	**0.5** (0.3)
SiO_2C_2	**−33** (−37)	**23** (36)	**0.8** (0.3)
$SiOC_3$	(−6)	(18)	(0.1)
SiC_4	**−10** (−3)	**24** (12)	**0.9** (0.0)
SiC_4 (asymmetric)	**−10** (−1)	**24** (30)	**0.9** (1.0)

recoupling times of τ = 6.7 and 9.3 ms should be dominated by DQ signals from ^{29}Si nearest-neighbors at ∼3.0−3.2 Å for Si−O−Si linkages and ∼3.2−3.4 Å for Si−C−Si linkages in the structure of SiOC PDCs. Moreover, no significant difference in the correlation peak pattern was observed with increased recoupling times (not shown), suggesting that these peaks in Figure 5 correspond predominantly to the connectivity between the nearest-neighbor Si atoms in the structure of the PDC. The peaks along the diagonal that correspond to the SiO_4, SiO_3C, SiO_2C_2, and SiC_4 structural units indicate that all these units are self-correlated, i.e., display connectivity between like units at the nearest-neighbor length scale. The strong cross-correlation peak between the SiO_4 and the SiO_3C units indicate that these two types of units are directly connected in the structure, while the appearance of the rather weak correlation peaks between the SiO_4 and the SiO_2C_2 units only at the longer recoupling time of 9.3 ms (Figure 5B), suggesting significantly less direct connectivity between them. It is likely that this correlation peak in Figure 5B results from SiO_2C_2 next-nearest neighbors connected to the SiO_4 units via the SiO_3C units. On the other hand, the minimal direct connectivity between the SiO_4 and the SiO_2C_2 units in the spectrum is consistent with the absence of a random connectivity between the SiO_xC_{4-x} units in the structure of this PDC. The complete absence of any cross-correlation between the SiO_4 and the SiC_4 units is also consistent with the chemical impossibility of any direct connectivity between these

https://dx.doi.org/10.1021/acs.jpcc.0c09860
J. Phys. Chem. C 2021, 125, 4777−4784

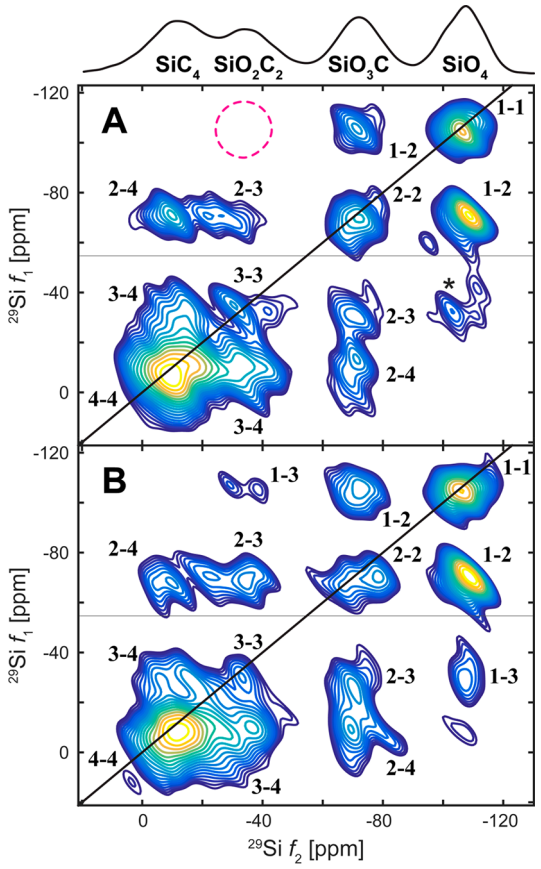

Figure 5. 2D ^{29}Si DQ correlation spectra collected with DQ excitation times of (A) 6.7 and (B) 9.3 ms, which were sheared along the indirect dimension to yield a SQ−SQ representation. Self- and cross-correlation peaks between various Si environments are indicated in the spectra, where SiO_4, SiO_3C, SiO_2C_2, and SiC_4 units are denoted as 1,2,3, and 4, respectively. The asterisk denotes a likely spinning sideband from the SiO_2C_2 (3) sites. The 1D ^{29}Si MAS spectrum in Figure 2 is reproduced on top of the 2D spectra.

units. Additionally, the correlation peak pattern in Figure 5 indicates significant connectivity between the SiO_3C units and all other units in the structure, including the high C-containing SiO_2C_2 and SiC_4 units, irrespective of the recoupling time. At the same time, the SiC_4 peak along the diagonal in Figure 5 shows a pronounced broadening, suggesting a strong preference toward self-connectivity and hence a spatial clustering.

In principle, it may be possible to go beyond this qualitative analysis of the 2D ^{29}Si DQ-SQ correlation spectrum and simulate the correlation peak intensities to obtain a more quantitative estimate of the average connectivity between the various nearest-neighbor SiO_xC_{4-x} units in the structure of the PDC. Such a simulation to a first-order approximation would be valid if (a) only the nearest-neighbor Si nuclei from the Si site of interest contribute to the DQ-SQ cross-peaks and (b) the ^{29}Si−^{29}Si dipolar couplings to each of the Si sites in this coordination sphere are all the same. However, it is not obvious whether either of these assumptions would be tenable since (a) it has been shown that the contributions to the correlation peaks from longer range distances, though smaller, do exist and (b) the variation of the ^{29}Si−^{29}Si dipolar coupling even within the nearest-neighbor sphere can be significant, introducing a large error in the simulations of cross-peak intensity. This could be an interesting avenue for a more in-depth investigation in future.

When taken together, these results provide a detailed picture of the structure of SiOC PDCs in terms of the spatial distribution and connectivity between the mixed-bonded SiO_xC_{4-x} units. The oxygen-rich SiOC network appears to consist of interconnected SiO_4 and SiO_3C tetrahedra, with the latter further connected to some SiO_2C_2 tetrahedra present as next-nearest neighbors of the SiO_4 units. Although the direct connectivity between the SiO_4 and the SiC_4 units is chemically prohibited, the avoidance of direct connectivity between the C-rich SiO_2C_2 units and the SiO_4 units is likely a result of the steric hindrance caused by the tetrahedral bonding displayed by both Si and C atoms in these units. Such avoidance is consistent with the previously reported fractal mass distribution of the Si atoms in the structure of SiOC PDCs with mixed bonding. No such bonding restriction is observed between the C-containing SiO_xC_{4-x} units. However, the strong preference for self-connectivity between the SiC_4 units, as mentioned above, implies the spatial clustering of these units, most likely at the interface between the SiOC network and the amorphous sp^2 C that is presumably present as either turbostratic carbon or graphene-like sheets. This interfacial clustering is expected to give rise to a mass distribution for these Si atoms that should have a significantly lower mass-fractal dimension D_f compared to those in the O-rich SiO_xC_{4-x} units. This expectation was indeed borne out experimentally, as previous studies reported that over a length scale on the order of ∼1 nm the oxygen-rich SiO_xC_{4-x} units exhibit D_f = 2.5, while the C-rich units display a lower value of D_f = 2.0 for the SiC_4 units.[9,34] The nearly two-dimensional mass distribution of the SiC_4 units is consistent with their role in the structure as the linking interfacial "tissue" between the tetrahedral SiOC network and the free-carbon nanodomains.[3] As mentioned above, this scenario is also consistent with the relatively large value of ^{29}Si Δ that was observed for the SiC_4 units (Table 1). In this regard, it is interesting note that a recent 3D transmission electron microscopic imaging study of a SiBOC PDC has shown that the sp^2 C planes are indeed bonded to Si−C nanodomains at their boundaries via Si−C covalent bonds that encase the silica-rich regions.[35]

Finally, an upper bound for the average diameter of oxygen-rich silica-like nanodomains in this PDC can be estimated by assuming a maximum avoidance in the connectivity between the SiO_4 and mixed-bonded SiO_xC_{4-x} units as well as noting that SiO_4 and SiO_3C units are present in a subequal (∼25−26%) concentration in the PDC. Considering the observation that the direct connectivity between the SiO_4 and the mixed-bonded SiO_xC_{4-x} units in this PDC is largely restricted to SiO_3C units, the silica-like nanodomains are expected to be terminated by SiO_3C units that decorate their surfaces. Therefore, if the surfaces of these nanodomains are defined by a shell of a single layer of SiO_4 tetrahedra (∼0.3 nm), and each of these tetrahedra in this shell is terminated by one SiO_3C unit on an average, then the average diameter of these domains would have to be ∼2.3 nm to yield subequal concentrations of the SiO_4 and SiO_3C units in this PDC.

SUMMARY

While the 1D ^{29}Si magic angle-spinning NMR spectrum of the SiOC PDC provides usual information on the relative fractions of the constituent SiO_xC_{4-x} tetrahedral units in the Si−O−C network, the full chemical shift tensor for each unit was

https://dx.doi.org/10.1021/acs.jpcc.0c09860
J. Phys. Chem. C 2021, 125, 4777−4784

obtained for the first time from a 2D ^{29}Si extended CSA amplification (xCSA) spectrum. A comparison between these experimental ^{29}Si chemical shift tensor parameters and those obtained from *ab initio* density functional theory-based calculations shows a good agreement in the δ_{iso} values and the increasing trend of $|\Delta|$ in the order SiO_2C_2 > SiO_3C > SiO_4. On the other hand, the unusually large experimental $|\Delta|$ value for the SiC_4 units likely originates from the linking of these units with the sp^2 C atoms in the free-carbon nanodomains at their interface with the Si−O−C network. The 2D ^{29}Si DQ-SQ correlation spectrum of this PDC indicates the extensive connectivity between the SiO_4 and SiO_3C units. On the other hand, direct linking between SiO_4 and SiO_2C_2 units appears to be largely avoided, possibly implying steric hindrance. No such avoidance in direct linking was observed for the C-containing SiO_xC_{4-x} units, although the strong self-correlation between the SiC_4 units suggests spatial clustering consistent with their role as the linking tissue between the tetrahedral Si−O−C network and the sp^2 C free-carbon nanodomains. Such steric hindrance to random connectivity between the constituent SiO_xC_{4-x} units and the spatial localization of the C-rich units is likely responsible for their fractal mass distribution, as determined in previous studies using ^{29}Si NMR SLR spectroscopy.

AUTHOR INFORMATION

Corresponding Author

Sabyasachi Sen − *Department of Materials Science & Engineering, University of California−Davis, Davis, California 95616, United States;* orcid.org/0000-0002-4504-3632; Email: sbsen@ucdavis.edu

Authors

Ivan Hung − *National High Magnetic Field Laboratory, Tallahassee, Florida 32310, United States;* orcid.org/0000-0001-8916-739X

Emanuel Ionescu − *Institute for Materials Science, Technische Universität Darmstadt, D-64287 Darmstadt, Germany*

Jishnu Sen − *Department of Computer Science, University of California−Los Angeles, Los Angeles, California 90095, United States*

Zhehong Gan − *National High Magnetic Field Laboratory, Tallahassee, Florida 32310, United States;* orcid.org/0000-0002-9855-5113

Complete contact information is available at: https://pubs.acs.org/10.1021/acs.jpcc.0c09860

Notes

The authors declare no competing financial interest.

ACKNOWLEDGMENTS

This study was supported by the National Science Foundation Grant NSF DMR-1855176. The National High Magnetic Field Laboratory (NHMFL) in Tallahassee, FL, USA, is supported through Grant NSF DMR-1644779 and the State of Florida.

REFERENCES

(1) Mera, G.; Navrotsky, A.; Sen, S.; Kleebe, H.-J.; Riedel, R. Polymer-Derived SiCN and SiOC Ceramics-Structure and Energetics at the Nanoscale. *J. Mater. Chem. A* **2013**, *1*, 3826−3836.

(2) Mera, G.; Riedel, R. Organosilicon-Based Polymers as Precursors for Ceramics. In *Polymer Derived Ceramics: From Nanostructure to Applications*; Colombo, P., Riedel, R., Soraru, G. D., Kleebe, H.-J., Eds.; DEStech Publications, Inc.: Lancaster, PA, 2009; pp 51−89.

(3) Colombo, P.; Mera, G.; Riedel, R.; Sorarù, G. D. Polymer-Derived Ceramics: 40 Years of Research and Innovation in Advanced Ceramics. *J. Am. Ceram. Soc.* **2010**, *93* (7), 1805−1837.

(4) Riedel, R.; Mera, G.; Hauser, R.; Klonczynski, A. Silicon-Based Polymer-Derived Ceramics: Synthesis Properties and Applications-A Review. *Nippon Seramikkusu Kyokai Gakujutsu Ronbunshi* **2006**, *114*, 425−444.

(5) Fiocco, L.; Li, S.; Stevens, M. M.; Bernardo, E.; Jones, J. R. Biocompatibility and Bioactivity of Porous Polymer-Derived Ca-Mg Silicate Ceramics. *Acta Biomater.* **2017**, *50*, 56−67.

(6) Ionescu, E.; Sen, S.; Mera, G.; Navrotsky, A. Structure, Energetics and Bioactivity of Silicon Oxycarbide-Based Amorphous Ceramics with Highly Connected Networks. *J. Eur. Ceram. Soc.* **2018**, *38*, 1311−1319.

(7) Stabler, C.; Ionescu, E.; Graczyk-Zajac, M.; Gonzalo-Juan, I.; Riedel, R. Silicon Oxycarbide Glasses and Glass-ceramics: "All-Rounder" Materials for Advanced Structural and Functional Applications. *J. Am. Ceram. Soc.* **2018**, *101*, 4817−4856.

(8) Rosenburg, F.; Balke, B.; Nicoloso, N.; Riedel, R.; Ionescu, E. Effect of the Content and Ordering of the sp^2 Free Carbon Phase on the Charge Carrier Transport in Polymer-Derived Silicon Oxycarbides. *Molecules* **2020**, *25*, 5919.

(9) Widgeon, S. J.; Sen, S.; Mera, G.; Ionescu, E.; Riedel, R.; Navrotsky, A. ^{29}Si and ^{13}C Solid-State NMR Spectroscopic Study of Nanometer-Scale Structure and Mass Fractal Characteristics of Amorphous Polymer Derived Silicon Oxycarbide Ceramics. *Chem. Mater.* **2010**, *22*, 6221−6228.

(10) Widgeon, S.; Mera, G.; Gao, Y.; Stoyanov, E.; Sen, S.; Navrotsky, A.; Riedel, R. Nanostructure and Energetics of Carbon-Rich SiCN Ceramics Derived from Polysilylcarbodiimides: Role of the Nanodomain Interfaces. *Chem. Mater.* **2012**, *24*, 1181−1191.

(11) Gregori, G.; Turquat, C.; Kleebe, H.-J.; Sorarù, G. D. Characterisation of SiCN/SiCO Glasses via SEM and TEM. *Key Eng. Mater.* **2001**, *206−213*, 2061−2064.

(12) Kleebe, H.-J.; Turquat, C.; Sorarù, G. D. Phase Separation in an SiCO Glass Studied by Transmission Electron Microscopy and Electron Energy-Loss Spectroscopy. *J. Am. Ceram. Soc.* **2001**, *84*, 1073−1080.

(13) Saha, A.; Raj, R.; Williamson, D. L.; Kleebe, H.-J. Characterization of Nanodomains in Polymer-Derived SiCN Ceramics Employing Multiple Techniques. *J. Am. Ceram. Soc.* **2005**, *88*, 232−234.

(14) Bréquel, H.; Parmentier, J.; Walter, S.; Badheka, R.; Trimmel, G.; Masse, S.; Latournerie, J.; Dempsey, P.; Turquat, C.; Desmartin-Chomel, A.; et al. Systematic Structural Characterization of the High-Temperature Behavior of Nearly Stoichiometric Silicon Oxycarbide Glasses. *Chem. Mater.* **2004**, *16*, 2585−2598.

(15) Turquat, C.; Kleebe, H.-J.; Gregori, G.; Walter, S.; Sorarù, G. D. Transmission Electron Microscopy and Electron Energy-Loss Spectroscopy Study of Nonstoichiometric Silicon-Carbon-Oxygen Glasses. *J. Am. Ceram. Soc.* **2001**, *84*, 2189−2196.

(16) Saha, A.; Raj, R.; Williamson, D. L. A Model for the Nanodomains in Polymer-Derived SiCO. *J. Am. Ceram. Soc.* **2006**, *89* (7), 2188−2195.

(17) Kleebe, H.-J.; Blum, Y. D. SiOC Ceramic with High Excess Free Carbon. *J. Eur. Ceram. Soc.* **2008**, *28*, 1037−1042.

(18) Mera, G.; Tamayo, A.; Nguyen, H.; Sen, S.; Riedel, R. Nanodomain Structure of Carbon-Rich Silicon Carbonitride Polymer-Derived Ceramics. *J. Am. Ceram. Soc.* **2010**, *93*, 1169−1175.

(19) Bai, W.; Widgeon, S.; Sen, S. Structure and Topological Characteristics of Amorphous Silicon Oxycarbide Networks: Results from Reverse Monte Carlo Simulations. *J. Non-Cryst. Solids* **2014**, *386*, 29−33.

(20) Marple, M.; Badger, J.; Hung, I.; Gan, Z.; Kovnir, K.; Sen, S. Structure of Amorphous Selenium by 2D ^{77}Se NMR Spectroscopy: An End to the Dilemma of Chain versus Ring. *Angew. Chem., Int. Ed.* **2017**, *56*, 9777−9781.

(21) Marple, M.; Hung, I.; Gan, Z.; Sen, S. Structural and Topological Evolution in Si_xSe_{1-x} Glasses: Results from 1D and 2D ^{29}Si and ^{77}Se NMR Spectroscopy. *J. Phys. Chem. B* **2017**, *121*, 4283−4292.
(22) Kaseman, D. C.; Hung, I.; Gan, Z.; Aitken, B.; Currie, S.; Sen, S. Structural and Topological Control on Physical Properties of Arsenic Selenide Glasses. *J. Phys. Chem. B* **2014**, *118* (8), 2284−2293.
(23) Hung, I.; Edwards, T.; Sen, S.; Gan, Z. MATPASS/CPMG: A Sensitivity Enhanced Magic-Angle Spinning Sideband Separation Experiment for Disordered Solids. *J. Magn. Reson.* **2012**, *221*, 103−109.
(24) Shao, L.; Yates, J. R.; Titman, J. J. Carbon-13 Chemical Shift Tensors of Disaccharides: Measurement, Computation and Assignment. *J. Phys. Chem. A* **2007**, *111*, 13126−13132.
(25) Hung, I.; Gan, Z. An Efficient Amplification Pulse Sequence for Measuring Chemical Shift Anisotropy under Fast Magic-Angle Spinning. *J. Magn. Reson.* **2011**, *213*, 196−199.
(26) Larsen, F. H.; Jakobsen, H. J.; Ellis, P. D.; Nielsen, N. C. Sensitivity-Enhanced Quadrupolar-Echo NMR of Half-Integer Quadrupolar Nuclei. Magnitudes and Relative Orientation of Chemical Shielding and Quadrupolar Coupling Tensors. *J. Phys. Chem. A* **1997**, *101*, 8597−8606.
(27) McNeill, S. A.; Gor'kov, P. L.; Shetty, K.; Brey, W. W.; Long, J. R. A Low-E Magic Angle Spinning Probe for Biological Solid State NMR at 750 MHz. *J. Magn. Reson.* **2009**, *197*, 135−144.
(28) Brouwer, D. H.; Kristiansen, P. E.; Fyfe, C. A.; Levitt, M. H. Symmetry-Based ^{29}Si Dipolar Recoupling Magic Angle Spinning NMR Spectroscopy: A New Method for Investigating Three-Dimensional Structures of Zeolite Frameworks. *J. Am. Chem. Soc.* **2005**, *127*, 542−543.
(29) States, D. J.; Haberkorn, R. A.; Ruben, D. J. A Two-Dimensional Nuclear Overhauser Experiment with Pure Absorption Phase in Four Quadrants. *J. Magn. Reson.* **1982**, *48* (2), 286−292.
(30) Bonhomme, C.; Gervais, C.; Babonneau, F.; Coelho, C.; Pourpoint, F.; Azaïs, T.; Ashbrook, S. E.; Griffin, J. M.; Yates, J. R.; Mauri, F.; et al. First-Principles Calculation of NMR Parameters Using the Gauge Including Projector Augmented Wave Method: A Chemist's Point of View. *Chem. Rev.* **2012**, *112*, 5733−5779.
(31) Schiţco, C.; et al. Silicon Oxycarbonitrides Synthesized By Ammonia-Assisted Thermolysis Route From Polymers: A Total X-ray scattering, Solid-state NMR, and TEM Structural Study. *J. Eur. Ceram. Soc.* **2016**, *36*, 979−989.
(32) Nimmo, J. P.; Kroll, P. First-Principles Calculations and Analysis of ^{29}Si Nuclear Magnetic Resonance Chemical Shifts in Silicon Oxycarbide Ceramics. *J. Phys. Chem. C* **2014**, *118*, 29952−29961.
(33) Hartman, J. S.; Berno, B.; Hazendonk, P.; Kirby, C. W.; Ye, E.; Zwanziger, J.; Bain, A. D. NMR Studies of Nitrogen Doping in the 4H Polytype of Silicon Carbide: Site Assignments and Spin-Lattice Relaxation. *J. Phys. Chem. C* **2009**, *113*, 15024−15036.
(34) Sen, S.; Widgeon, S. On the Mass Fractal Character of Si-Based Structural Networks in Amorphous Polymer Derived Ceramics. *Nanomaterials* **2015**, *5* (1), 366−375.
(35) Moldovan, S.; Ersen, O.; Sanchez, C.; Campostrini, R.; Sorarù, G. D. Shedding light onto the nano- and micro-structures of B-containing SiOC glasses using high resolution TEM 3D imaging. *J. Eur. Ceram. Soc.* **2019**, *39*, 3042−3050.

https://dx.doi.org/10.1021/acs.jpcc.0c09860
J. Phys. Chem. C 2021, 125, 4777−4784